Journal of Materials Chemistry C

Accepted Manuscript

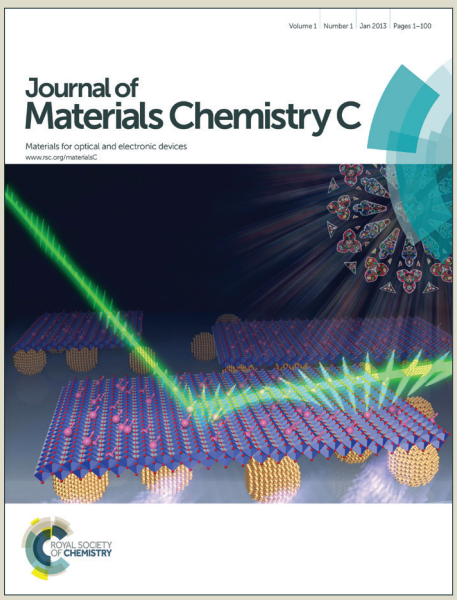

ROYAL SOCIETY OF CHEMISTRY

www.rsc.org/materialsC

Graphical abstract

The Y_2O_3 films grown with a new liquid Y precursor, $(iPrCp)_2Y(iPr\text{-}amd)$, have been investigated with chemical properties of precursor, atomic layer deposition (ALD) process, and material characterization of the deposited film and its non-volatile resistive switching behavior. A heteroleptic $(iPrCp)_2Y(iPr\text{-}amd)$ has been synthesized so that it exist in liquid phase at room temperature. The vapor pressure of 1 Torr is obtained at 168 ℃, and thermal evaporation and decomposition begins from 250 ℃ and 425 ℃, respectively. Y_2O_3 film is fabricated by ALD technique using $(iPrCp)_2Y(iPr\text{-}amd)$ and water. The growth of Y_2O_3 film is well self-limited, the ALD window is from 350 ℃ to 450 ℃, and the growth rate is 0.06 nm/cycle. The deposited Y_2O_3 film reveals polycrystalline cubic structure, higher refractive index over 1.8 at 632.8 nm, and high dielectric constant of 24. The as-deposited Y_2O_3 film is very compositionally stoichiometric and constant with Y and O through depth and also includes small -OH bonding in the film without any additional processes. The $Ru/Y_2O_3/Ru$ resistor shows a resistance switching between low and high resistance states with voltage sweeping and the resistance ratio between two states is over 1,000 times preferable to non-volatile memory operation.

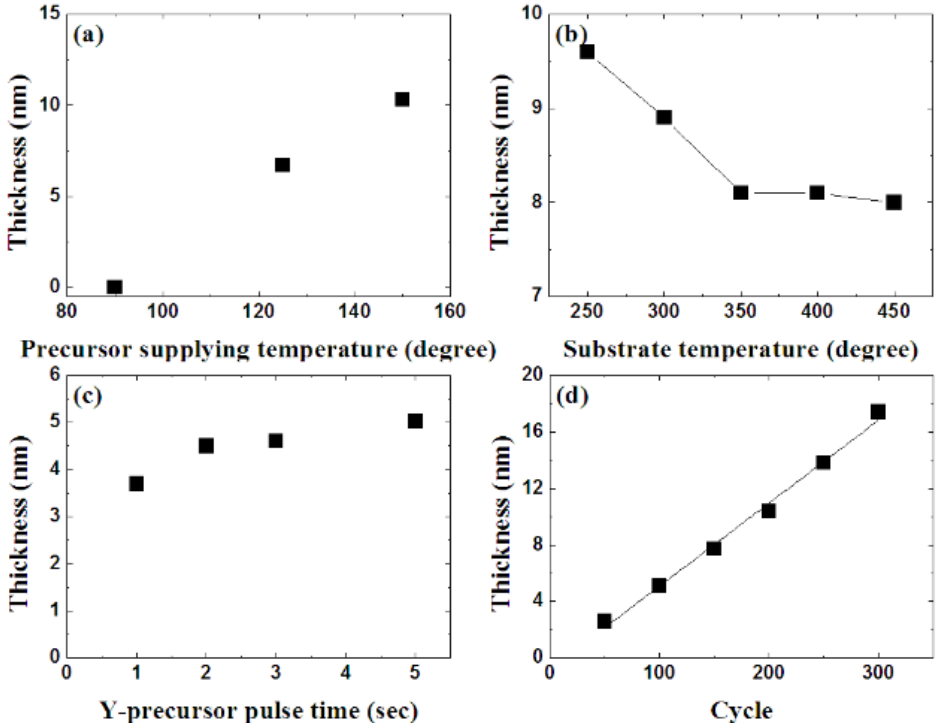

Journal of Materials Chemistry C

RSCPublishing

ARTICLE

Atomic layer deposition of Y_2O_3 films using hetroleptic liquid $(iPrCp)_2Y(iPr\text{-}amd)$ precursor

Cite this: DOI: 10.1039/x0xx00000x

In-Sung Park,[ab] Yong Chan Jung,[a] Sejong Seong,[a] Jinho Ahn,*[a] Jiehun Kang,[c] Wontae Noh[d] and Clement Lansalot-Matras[d]

Received 00th June 2014,
Accepted 00th January 2014

DOI: 10.1039/x0xx00000x

www.rsc.org/

The Y_2O_3 films grown with a new liquid Y precursor, $(iPrCp)_2Y(iPr\text{-}amd)$, have been investigated with chemical properties of precursor, atomic layer deposition (ALD) process, and material characterization of the deposited film and its non-volatile resistive switching behavior. A heteroleptic $(iPrCp)_2Y(iPr\text{-}amd)$ has been synthesized so that it exist in liquid phase at room temperature. The vapor pressure of 1 Torr is obtained at 168 °C, and thermal evaporation and decomposition begins from 250 °C and 425 °C, respectively. Y_2O_3 film is fabricated by ALD technique using $(iPrCp)_2Y(iPr\text{-}amd)$ and water. The growth of Y_2O_3 film is well self-limited, the ALD window is from 350 °C to 450 °C, and the growth rate is 0.06 nm/cycle. The deposited Y_2O_3 film reveals polycrystalline cubic structure, higher refractive index over 1.8 at 632.8 nm, and high dielectric constant of 24. The as-deposited Y_2O_3 film is very compositionally stoichiometric and constant with Y and O through depth and also includes small -OH bonding in the film without any additional processes. The $Ru/Y_2O_3/Ru$ resistor shows a resistance switching between low and high resistance states with voltage sweeping and the resistance ratio between two states is over 1,000 times preferable to non-volatile memory operation.

Introduction

In recent years, yittrium oxide (Y_2O_3) film has attracted considerable attention for its wide range of application. The excellent material properties of Y_2O_3 film are allowed it to be applied to various electronic and optoelectronic devices. There are a lot of applications of Y_2O_3: metal-oxide-semiconductor field effect transistors (MOSFET) and carbon-based FET,[1,2] non-volatile memory,[3,4] laser,[5,6,] phosphor,[7,8] superconductor,[9] and solid oxide fuel cell (SOFC).[10-12] As a gate dielectric in FET, Y_2O_3 is one of the most promising candidates to substitute SiO_2 layer due to its medium dielectric constant (15), wide bandgap (5.6 eV), low leakage current, high breakdown voltage, large conduction band offset (2.3 eV), and good thermal stability.[1] In addition, Y_2O_3 can be used as an insulating layer of metal-insulator-metal (MIM) structure in non-volatile resistive switching memory. Excellent device characteristics have been revealed such as high resistance ratio, nondestructive readout, and good data retention.[3] The rare earth (RE)-doped Y_2O_3 films, $Er:Y_2O_3$, $Er:Eu:Y_2O_3$, and $Er:Yb:Y_2O_3$, are used as laser hosts because they have high transparency, refractive index (1.7-1.9), mechanical strength, thermal conductivity, and good compatibility with Si technologies.[5] The RE-doped Y_2O_3 films have been widely used to photonic and electric devices, namely, optical amplifiers, sensors, upconverters, light emitting diode (LED), organic LED, and thin film electroluminescent applications.[8,13,14] Y_2O_3 is also used to make high temperature superconductor YBa_2Cu_3O.[9] The Y_2O_3-based films such as yttria-stabilized zirconia (YSZ)[11] and yttria-doped ceria (YDC)[12] films are applied as solid-state electrolytes to SOFC.

Atomic layer deposition (ALD) is a relatively new technology for thin film formation, but it has been frequently employed in various nano-device fabrications and become one of the leading film deposition methods.[15-19] In ALD process, the film grows through a unique surface reaction of vaporized precursors that are alternately supplied into the substrate surface. For binary metal oxide formation, the complete cycle of ALD for a monolayer growth is consisted of pulse of metal precursor, inert gas purge, pulse of oxidant, and inert gas purge. Each provided precursor should be well isolated to prevent the gas-phase reaction. The significant advantage of the ALD process is the self-limiting growth of monolayer. In spite of slow growth, ALD has offered high quality thin films, good controllability of the thickness in atomic-level, thickness uniformity, and perfect conformal coating on complex-structured surfaces.[16]

The choice of proper metal precursor is very crucial for successful ALD process. The main requirements of metal precursors are high vapor pressure (more than 0.1 Torr) at its supplying temperature, no self-decomposition at process temperature, and aggressive reaction with ligands on surface. Thermal and plasma-assisted ALD techniques with various types of precursors have been used to deposit pure, Y-doped, and ion-doped Y_2O_3 films.[12,20-23] The ALD processes with the precursors with O-, N-, and C-coordinated ligands and their heteroleptic ligands have been reported.[12,20-28]

Among O-coordinated ligands, β-diketonate precursors are thermally stable. The tris(2,2,6,6-tetramethyl-3,5-hemptadione) yttrium, $Y(thd)_3$, has been used to fabricate Y_2O_3,[20] $YScO_3$,[21], YSZ,[22], YF_3,[23] and YDC[12] thin films. The solid $Y(thd)_3$ should be sublimated at 125 °C to achieve optimal ALD condition.[12] The ALD window using the $Y(thd)_3$ precursor and ozone results in the temperature range of 250-375 °C but with low growth rate of 0.23 Å/cycle.[20] The impurity level of grown films, however, is very high. Impurity carbon and hydrogen levels are as high as 1.0-1.4 at.% and 1.3-1.7 at.%, respectively, even the deposition is carried out at 350 ℃ in the high edge of ALD window.

N-coordinated precursors approach instead, has been demonstrated

lower carbon level in the films. The yttrium tris(*N*,*N*'-diisopropylacetamidinate), $Y(iPr_2\text{-amd})_3$, with H_2O has been used and it is obtained the proper growth rate of 0.8 Å/cycle within the temperature range of 150-280 ℃.[24] The impurity levels of carbon and nitrogen are reduced below 0.5 at. %. The ratio of Y to O, however, is close to 1:2. Even worse is that hygroscopic Y_2O_3 films adsorb water very easily after air exposure, showing large amount of Y-OH states in XPS analysis. Therefore, to prevent or to reduce water adsorption in Y_2O_3 film, additional *in-situ* deposition of an Al_2O_3 capping layer or thermal annealing at 400 °C is required to keep good dielectric and electrical characteristics.

Recently the cyclopentadienyl (Cp = C_5H_5)-based precursors such as YCp_3,[25] $Y(MeCp)_3$,[11,25] $Y(EtCp)_3$,[26,27] and $Y(iPrCp)_3$[28] have been used in ALD process. Those Cp-based precursors are much more reactive with water than O-coordinated ligands, leading to higher growth rate. The growth rate of Y_2O_3 film with Cp-based precursors/H_2O (1.2-1.8 A/cycle),[25] is about 5 or 8 times larger than that with $Y(thd)_3/O_3$ process (0.23 A/cycle).[20] Y_2O_3 films using $Y(EtCp)_3$ and H_2O show relatively lower carbon ratio (< 0.5 %) and good stoichiometric property (Y:O = 2:3), but its ALD process window is too narrow (250-285 ℃). Narrow ALD window is also found in $Y(MeCp)_3$-based Y_2O_3 films within the temperature range of 250-300 °C with constant growth rate of 1.2-1.3 Å/cycle. The narrow ALD windows hinder to apply Cp-based precursors to diverse application. In addition, the low thermal stability of Cp-based precursors prevents them from using in ALD.

The described ALD-Y_2O_3 films contain higher impurities such as C- and -OH bonds because they are deposited at relatively lower temperature. Most of Y precursors so far are solid-based complex and they have been adopted because of easy synthesis and handling. Unsublimated solid precursors from the source canister, however, often remain in precursor-supply-line and in an ALD chamber, provoking detrimental defects in the films and contamination in ALD system. Since usual solid precursors are not generally much reactive towards water, it is essential to react with aggressive oxidants like ozone or plasma reactive oxygen but results in lower growth rate. Therefore, to solve these problems of solid precursors, the liquid precursors are preferred in ALD process if it is available. The precursors such as $Y(EtCp)_3$ is liquid phase at its vaporization temperature of 120 ℃[26] and for $Y(iPrCp)_3$ is melted at 55 ℃.[28] In recent, the heteroleptic precursors showing liquid phase at room temperature have been used in ALD processes.[29,30]

In this study, a novel heteroleptic Y precursor which is liquid at room temperature, $(iPrCp)_2Y(iPr\text{-amd})$, has been synthesized and its chemical and thermal properties are analyzed. Within our knowledge, this liquid precursor is the first successful fabrication. The ALD process conditions to fabricate Y_2O_3 films are investigated and optimized. The structural, optical, and chemical properties of grown films are characterized. Finally, the dielectric and electrical properties are characterized using metal-oxide-Si (MOS) capacitor and MIM non-volatile memory, respectively.

Experimental

Synthesis of $(iPrCp)_2Y(iPr\text{-amd})$ precursor

The yttrium precursor, $(iPrCp)_2Y(iPr\text{-amd})$, was prepared in relatively high yield by a reaction of $Y(iPrCp)_3$ with one equivalent of iPr-amd-H in pentane at room temperature, followed by vacuum distillation. A solution of $Y(iPrCp)_3$ (130 g, 316 mmol) in *ca*. 200 mL pentane at room temperature was added to a solution of iPr-amd-H (45 g, 316 mmol) in *ca*. 200 mL pentane dropwise over 30 min. Raw pentane purchased from Sigma Aldrich was used as received without any further purification. The $Y(iPrCp)_3$ and iPr-amd-H were also obtained commercially and used as received. The mixture was stirred at room temperature overnight. The solvent and volatiles were evaporated under vacuum. The resulting yellow oil was vacuum distilled at 145-150 ℃ at 70 mTorr. The yield of $(iPrCp)_2Y(iPr\text{-amd})$ is 82 % (116 g).

Characterization of $(iPrCp)_2Y(iPr\text{-amd})$ precursor

To identify the compound formation of $(iPrCp)_2Y(iPr\text{-amd})$, the ^1H nuclear magnetic resonance (NMR) spectra were recorded on a Bruker Avance II spectrometer at 400 MHz in benzene-d_6 solvent. The chemical shifts were reported in relative to tetramethylsilane (TMS). The vapor pressure and the thermal properties of $(iPrCp)_2Y(iPr\text{-amd})$ were measured on Mettler Toledo thermogravimetry analyzer (TGA) and differential scanning calorimetry (DSC). All experiments were performed under vacuum or under nitrogen atmosphere.

ALD process for Y_2O_3 film with $(iPrCp)_2Y(iPr\text{-amd})$

Y_2O_3 films were prepared in a flow-type ALD reactor (CN1 Co.) using a liquid $(iPrCp)_2Y(iPr\text{-amd})$ precursor and H_2O as metal precursor and oxidant, respectively. Prior to ALD-Y_2O_3 film growth, the B-doped Si (100) substrates were cleaned with dilute HF solution and deionized water to remove the native oxide. For the optimum Y_2O_3 deposition, the precursor supplying temperature (90-150 °C), substrate temperature (150-450 °C), and Y pulse time were varied. The $(iPrCp)_2Y(iPr\text{-amd})$ precursor was supplied into the reactor using nitrogen as a carrier gas. The water at room temperature was supplied into reactor without any carrier gas flow.

Characterization of deposited Y_2O_3 films

Thickness and refractive index of ALD-Y_2O_3 film on Si substrate were measured using a TEM (JEOL JEM-2010) and a spectroscopic ellipsometry (Horiba UVISEL). Crystallinity of the film was identified using an X-ray diffractometer (XRD, Rigaku D/MAX 2500/PC). The surface was checked by atomic force microscopy (AFM). The X-ray photoelectron spectroscopy (XPS, Thermo Scientific-Theta Probe) analyzed the chemical binding of the Y_2O_3 films. The Auger electron spectroscopy (AES) system (PHI 700Xi) was used to analyze the depth profile of composition.

Dielectric and electrical properties of ALD-Y_2O_3 film

To evaluate the dielectric and electrical parameters of ALD-Y_2O_3 films, two types of test vehicle devices, which are Ru/Y_2O_3/Si MOS capacitor and Ru/Y_2O_3/Ru/Si resistor with MIM structure, were fabricated. The Ru metal was deposited with a dc sputtering at room temperature. The top electrodes of both devices were defined using an aligner system and conventional liftoff method. The capacitance-voltage (C-V) measurements were performed with a HP4284 LCR meter for MOS capacitor. The capacitance was measured by sweeping from +2 V to -2 V and then vice versa. The capacitance equivalent thickness (CET) of the MOS capacitor was determined with the saturated capacitance at -2 V in C-V curves measured at 100 kHz. Using current-voltage (I-V) curves measured by using a HP 4155 semiconductor parameter analyzer, the resistive switching behavior of MIM resistor was obtained. The voltage of top electrode was varied by positive and negative value increment from 0 V and all measurements were carried out separately.

Results and discussion

Chemical identification of $(iPrCp)_2Y(iPr\text{-amd})$

Fig. 1 depicts the ^1H NMR spectra of synthesized $(iPrCp)_2Y(iPr\text{-amd})$ and the corresponding precursor; the methyl groups of the iso-propyl substituent on the cyclopentadienyl ring appears at 0.99 ppm as a

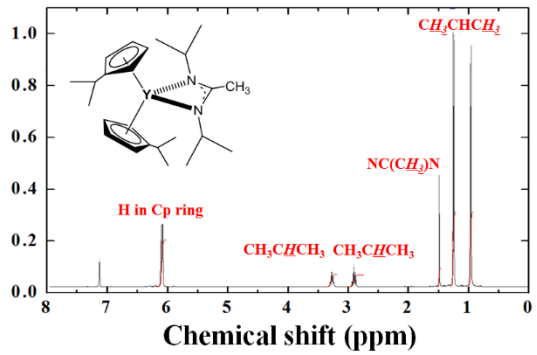

Fig. 1. ^{1}H NMR spectra of synthesized $(iPrCp)_2Y(iPr\text{-}amd)$ and its corresponding schematic picture.

doublet but the other methyl groups on the amidinate also show doublet at 1.27 ppm. Each proton on the iso-propyl group shows multiplets coupled with the neighbor two methyl groups at 2.92 ppm for the iso-propyl substituent on the ring and at 3.30 ppm for the one on the amidinate, respectively. The backbone methyl group appears at 1.51 ppm as a singlet. The ring photons appear at around 6.12 ppm. The peak at 7.6 ppm comes from solvent.

Thermal properties of $(iPrCp)_2Y(iPr\text{-}amd)$

Fig. 2 shows the vapor pressure variation of $(iPrCp)_2Y(iPr\text{-}amd)$ precursor with temperature. The synthesized $(iPrCp)_2Y(iPr\text{-}amd)$ precursor is a yellow oil that has vapor pressure of 1 Torr at around 168 °C. It is quite interesting that the precursor is in a liquid phase at room temperature, has not been available. Owing to the atomic size of yttrium, bulky ligands are usually required to cover the metal and to stabilize the precursor, thus the formation of solid cannot be avoided. The $(iPrCp)_2Y(iPr\text{-}amd)$ precursor can exist in liquid phase owing to its heteroleptic nature of the precursor.[30]

Moreover, it has good thermal stability so that it can evaporate without decomposition in TGA experiment up to 500 °C, showing one step profile in Fig. 3. In Fig. 3, the precursor shows that evaporation begins to occur 250 °C in single step till 320 °C with very low residual mass of about 0 %. This means no decomposition during evaporation. Also, the absence of residual mass amounts reveals better thermal stability of molecule than other precursors at higher temperature.

To investigate the behavior of molecules at higher temperatures in ALD process, DSC analysis is presented in Fig. 4. In DSC analysis, it begins to deform from 375 °C and start to rapidly decompose at 425 °C, which indicates the decomposition to be exothermic reaction.

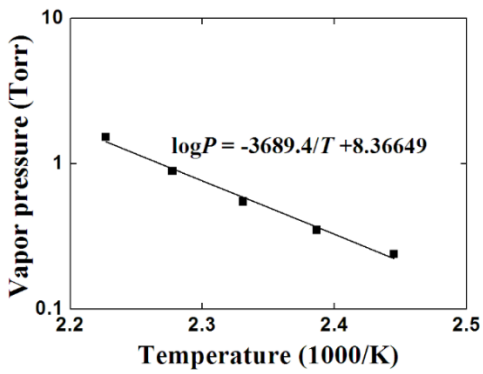

Fig. 2. Vapor pressure variation of $(iPrCp)_2Y(iPr\text{-}amd)$ with temperature.

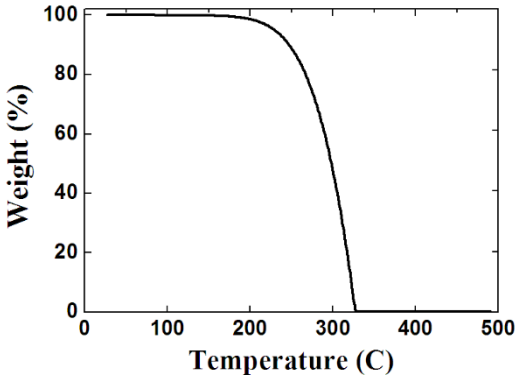

Fig. 3. TGA curve of $(iPrCp)_2Y(iPr\text{-}amd)$ precursor.

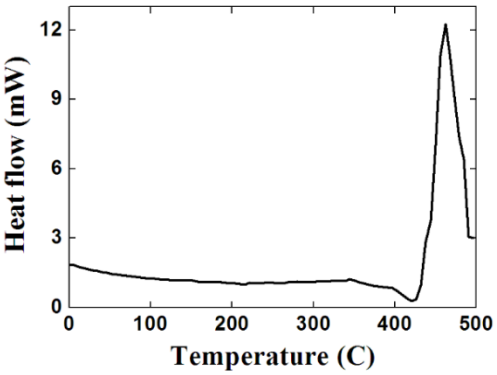

Fig. 4. DSC measurement of $(iPrCp)_2Y(iPr\text{-}amd)$ precursor.

The decomposition at relatively high temperature demonstrates that $(iPrCp)_2Y(iPr\text{-}amd)$ indicates its thermal stability. The melting point is not detected in this measurement range.

ALD of Y_2O_3 film with $(iPrCp)_2Y(iPr\text{-}amd)$ precursor

In ALD process, the metal precursor should be evaporated and sufficient amount is to be supplied into the chamber for monolayer coverage. One parameter acquired adequate ALD process is the overall precursor exposure on the growth surface. The exposure amount depends on the partial pressure of the used precursor and its pulse time. Practically, the partial pressure of precursor in reactor can be controlled by the precursor supply temperature and the flow rate of carrier gas. To supply appropriate amount of liquid $(iPrCp)_2Y(iPr\text{-}amd)$ precursor, film thickness with ALD 150 cycles is investigated by varying the precursor supplying temperature with the fixed pulse time of 3 sec at substrate of 350 °C . Fig. 5a shows the growth results with Y precursor supplying temperature. When the precursor is supplied at 85 °C (0.01 Torr), no growth is observed because the vapor pressure is too low to vaporize $(iPrCp)_2Y(iPr\text{-}amd)$. Moreover, when the precursor canister is kept at 125 °C and furnished with the same process cycles, Y_2O_3 film has been grown around 7 nm. However, the most appropriate growth thicker than 10 nm is appeared at 150 °C precursor supplying temperature (0.4 Torr). The liquid $(iPrCp)_2Y(iPr\text{-}amd)$ precursor is so thermally stable up to 250 °C in TGA result that this temperature is stable enough as precursor supplying temperature. The $(iPrCp)_2Y(iPr\text{-}amd)$ supplying temperature is fixed at 150 °C.

In Fig. 5b, the ALD process temperature window with $(iPrCp)_2Y(iPr\text{-}amd)$ precursor is characterized by the thickness change as function of substrate temperature from 250 °C to 450 °C under optimized exposure which is 3 sec pulse for $(iPrCp)_2Y(iPr\text{-}amd)$ and 0.2 sec for

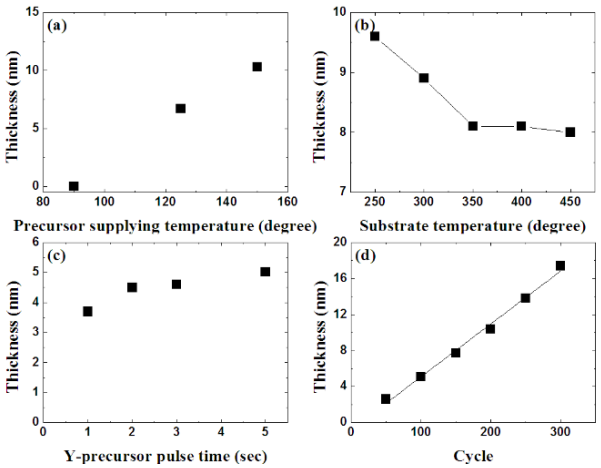

Fig. 5. Growth thickness of Y_2O_3 film with (a) $(iPrCp)_2Y(iPr\text{-}amd)$ precursor supplying temperature, (b) with substrate temperature, (c) with $(iPrCp)_2Y(iPr\text{-}amd)$ precursor pulse time, and (d) with ALD cycle with the growth rate (slope) of 0.06 nm/cycle. The H_2O pulse time is 0.2 sec for all of Y_2O_3 deposition.

H_2O. The ALD window is temperature range with constant deposited thickness and that is a favorable feature of an ALD process. In our study, the region of constant growth has been observed as high as 350 °C to 450 °C. According to DSC result, $(iPrCp)_2Y(iPr\text{-}amd)$ is not self-decomposed in the temperature range. Therefore, an ALD process is performed when the substrate temperature is higher than 350 °C. It is relatively high temperature ALD window. For examples, ALD window for Y_2O_3 film is 250-350 ℃ with $Y(thd)_3$,[20] 150-280 °C with $Y(iPr_2\text{-}amd)_3$,[24] 200-400 °C with $Y(MeCp)_3$,[25] 250-285 °C with $Y(EtCp)_3$,[26] and 245-300 °C with $Y(iPrCp)_3$.[28] The higher ALD window is related to the higher decomposition temperature revealed in DSC measurement. The ALD at higher process temperature makes the advantages on the grown film dense and less contamination with C, N, and H.

Fig. 5c is the saturation curve of Y precursor with precursor supplying time at 350 °C of substrate temperature. The figure represents self-limited growth after 2 sec. With the proper ALD process conditions, Y_2O_3 films are deposited with cycle variation. Therefore, the deposition has been carried out at 350 °C of substrate temperature with $(iPrCp)_2Y(iPr\text{-}amd)$ pulse time of 3 sec supplied at 150 °C and H_2O pulsing of 0.2 sec at room temperature. As can be seen in Fig. 5d, the thickness of Y_2O_3 film is linearly increased with the number of process cycle. The growth rate of Y_2O_3 deposition was 0.06 nm/cycle. Y_2O_3 deposition on Si substrate reveals almost 1.3 nm nucleation delay. The incubation cycle is usual with the case of H_2O oxidant use whilst no incubation in the case of O_3 reactant.[20,28] The difference between them is originated from the reaction mechanism between oxidant and underlying surface. The incubation cycle is the time until the substitution from -H termination on Si substrate to –OH fully.

Crystalline Y_2O_3 film

The crystal structure of the 30-nm-thick Y_2O_3 film on p-type Si substrate is determined by XRD. Most of diffraction peaks corresponds to the cubic phase of Y_2O_3 (JCPDS 41-1105). Fig. 6 demonstrates that the normal direction of (222) plane in Y_2O_3 film is preferably oriented perpendicular to the surface of Si (100) substrate. The (400), (332), (431), (440), and (622) planes of cubic Y_2O_3 are also observed. The preceding results show that Y_2O_3 film on Si substrate using thermal ALD method has also a cubic structure due to the high

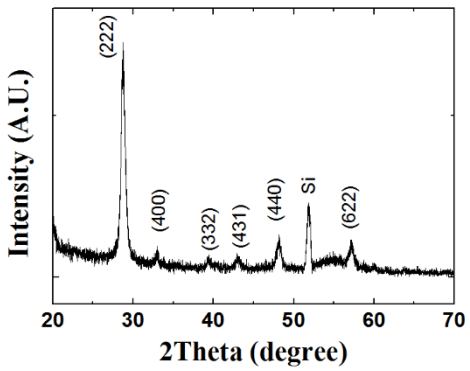

Fig. 6. XRD patterns of Y_2O_3 films deposited at 350 °C on Si.

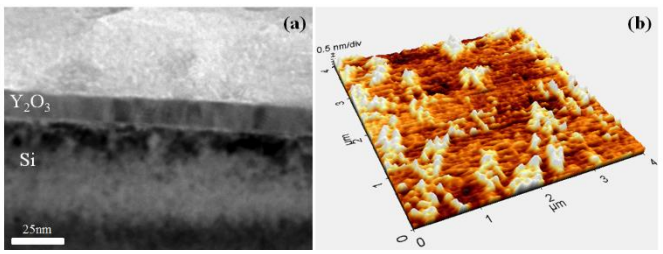

Fig. 7. (a) TEM image of Y_2O_3 films deposited on Si substrate with 13.3 nm and (b) its AFM image with RMS of 0.39 nm.

reactivity of Y precursor.[24-27] The dominant plane of ALD-Y_2O_3 films is (222) or (400) along with precursor and deposition temperature. The Y_2O_3 films using YCp_3 and H_2O at 200-350 °C show the crystal structure with preferred (400) plane but at 400 °C the strongest is changed to (222).[25] With the more reactive precursor of $Y(MeCp)_3$, (222) reflection is obtained from Y_2O_3 film deposited at 175 ℃. The crystal structure in which (222) plane is preferably stacked parallel to substrate indicates that $(iPrCp)_2Y(iPr\text{-}amd)$ is adequately reactive with H_2O and high reactivity of precursor allows the Y_2O_3 film to grow in crystalline form. Fig. 7a shows a TEM images Y_2O_3 film on Si substrate. The thickness of Y_2O_3 film is uniform and average 13.3 nm thick. It is also found that the top surface of Y_2O_3 films is so smooth. The surface morphology of the film is analyzed by AFM. The root mean square (RMS) of this film is found to be 0.39 nm as shown in Fig. 7b.

Chemical bonding and elemental analysis in Y_2O_3 film

Fig. 8 presents the XPS spectra of Y 3d and O 1s for deposited Y_2O_3 film at 350 °C. In Fig. 8a, the appearing two main peaks at 156.2 eV and 158.2 eV ($3d_{5/2}$ and $3d_{3/2}$) show stoichiometric Y_2O_3 oxide.[31-33] If there is hydroxylation in the films which essentially need post thermal treatment after film processing, XPS spectra usually shows two key features; the binding energy of both Y 3d and O 1s are shifted to higher side by around 0.6-1.8 eV, which can be back to normal position after annealing and the intensity of lower binding energy peak is stronger than higher energy peak.[34-36] Contrast to several studies, which reported hydroxylation formation is inevitable,[24,36] XPS result in this study shows no appreciable binding energy shift, suggesting that no hydroxylation (Y-OH) or less than spectrometer detection limit in the film. Even the similar structured but still solid phase precursor $Y(iPrCp)_3$ shows thick hydroxylation from the surface to deep inside, being compared against our result.[28] It suggests that liquid $(iPrCp)_2Y(iPr\text{-}amd)$ precursor approach to avoid water absorption during deposition process or air exposure successfully forms good

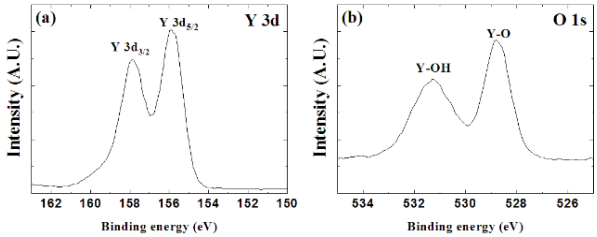

Fig. 8. XPS spectra of Y_2O_3 film for (a) Y 3d and (b) O1s.

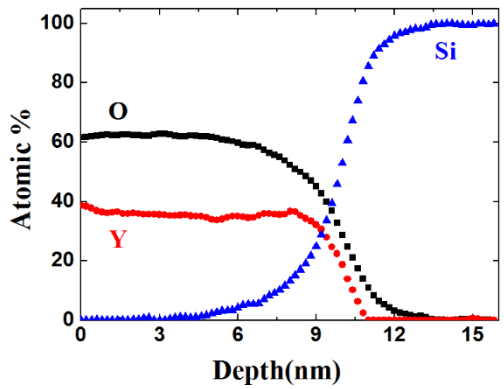

Fig. 9. Depth profile of Y_2O_3 film measured by AES.

structured oxide without subsequent heat treatment or forming capping layer.

The O 1s spectra of Y_2O_3 film are also composed two main peaks at 529.1 eV and 531.6 eV.[31,32] The lower peak at 529.1 eV is stronger than the higher energy peak and is originated from stoichiometric Y_2O_3 film, which is well consistent with Y 3d spectra.[34] The peak at 531.6 eV is broader but weaker, implying multiple bonding features such as -O-C due to contamination of air exposure before loading to XPS analysis, -O-H due to water absorption, and -Si-O-Y in the interface layer.[34] The C 1s binding energy (not shown) is found at 284.9 eV and 288.9 eV corresponds adventitious carbon and carbonates, respectively.[32] Since the Y_2O_3 film thickness is thick enough (~ 30 nm) and no trace of the characteristic feature of SiO_2 at ~ 533 eV, the emission from possible interfacial silicate or SiO_2 may be small.[37] The most reliable assignment to the high energy peak can be attributed to small mixture of various contributions from -O-C and -O-H.[36] Typical assignment of the high binding energy component has been to Y-OH formation during ALD deposition process or air exposure if there is clear binding energy shift as in Y 3d emission.[24] To reduce water adsorption in Y_2O_3 film after air exposure, an additional deposition of an Al_2O_3 capping layer or thermal annealing is required.[24] As discussed above, any additional processes such as capping layer or thermal heat treatment are not necessary with $(iPrCp)_2Y(iPr\text{-}amd)$ since the hydroxylation formation by solid precursor and the contamination from air moisture can be avoided. No appreciable binding energy shift in all the O 1s spectra, again, is found as in the case of Y 3d. This demonstrates liquid phase precursor $(iPrCp)_2Y(iPr\text{-}amd)$ approach is more advantageous to avoid Y-OH formation than conventional solid phase precursor.[24,28,34] The atomic ratio of Y/O in Y_2O_3 film is extracted by XPS analysis. The Y/O ratio is 0.62, which the value is the same with the stoichiometric Y_2O_3 film grown at 350-375 °C with $Y(thd)_3$ and O_3.[20] The Y/O ratio, from the

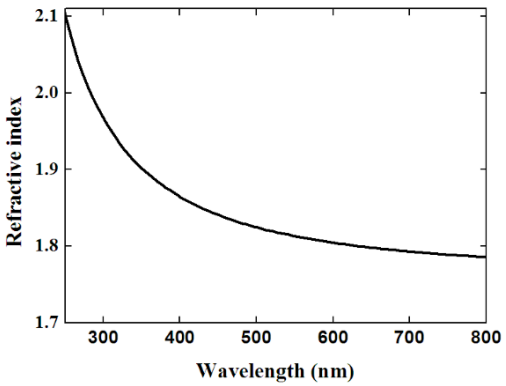

Fig. 10. Refractive index of Y_2O_3 film.

Auger depth profiling analysis in Fig. 9, is well maintained in almost constant through depth, which further supports good stoichiometric quality of the film.

Optical property of Y_2O_3 film

In visible region of light, Y_2O_3 films are characterized by a high refractive index which allows them to be applied to optical devices.[28,38] The refractive index of Y_2O_3 film is strongly dependent on the fabrication methods, process temperature, and crystalline structure. The refractive index can be determined using the Lorentz oscillator formula. Fig. 10 shows it as the function of wavelength from 250 nm to 830 nm. For the precise analysis, the thickness of Y_2O_3 film is obtained from TEM measurement. It is found that the higher refractive index of ALD-Y_2O_3 film processed with $(iPrCp)_2Y(iPr\text{-}amd)$ is obtained. The extracted value at 632.8 nm wavelength is over 1.8. The refractive index of ALD-Y_2O_3 film using a $Y(iPr_2\text{-}amd)_3$ is about 1.8 at 632.8 nm[24] and that of ALD-Y_2O_3 film processed at 250 ℃ using a $Y(iPrCp)_3$ precursor is 1.77 and anneal at 600 ℃ and 800 ℃ are 1.79 and 1.88, respectively.[28] The higher refractive index means the higher density and dielectric constant. The dense Y_2O_3 film deposited with $(iPrCp)_2Y(iPr\text{-}amd)$ can prevent from absorbing water vapor in air, which is well demonstrated in XPS results.

Dielectric property of Y_2O_3 film

The dielectric constant of Y_2O_3 film is evaluated from the C-V curves of MOS capacitor. The typical C-V curves of Ru/Y_2O_3/Si capacitors are presented in Fig. 11a with Y_2O_3 films of 10 nm, 20 nm, and 30 nm thick. As Y_2O_3 films become thinner, the distortions in C-V curves are observed due to the large density of slow interface states.[39] The saturated capacitance values of MOS capacitors are 10.8 fF/μm^2, 7.6 fF/μm^2, and 5.4 fF/μm^2 respectively. Using those capacitance values,

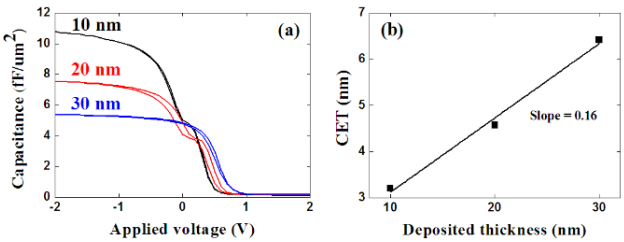

Fig. 11. (a) C-V curves of Ru/Y_2O_3/Si MOS capacitors with the thickness of Y_2O_3 films and (b) their CET variation with film thickness. The slope in (b) is reciprocally related to the dielectric constant of 24.

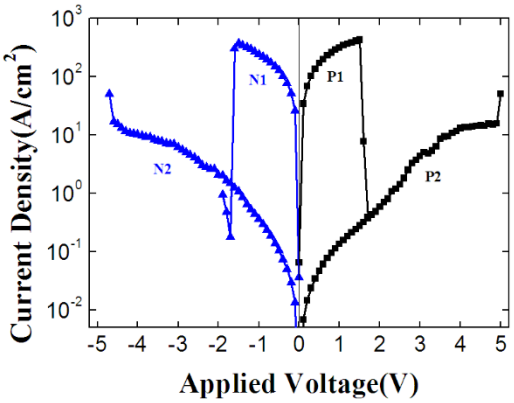

Fig. 12. The J-V curves of Y_2O_3 films. The sweeps are independently executed positive (P1 and P2) and negative (N1 and N2) voltage stress. P1(N1) sweep is followed by P2(N2).

each CET is obtained. The CET variation with the thickness of Y_2O_3 film is drawn in Fig. 11b. From the slope, dielectric constant of Y_2O_3 film is evaluated as 24. The higher dielectric constant is well compatible with the higher refractive index and the density.

Resistive switching behaviors with Y_2O_3 film

To investigate the electrical property, in particular, resistive switching, I-V measurements are carried out on Ru/Y_2O_3/Ru/Si MIM structures with 30 nm insulating Y_2O_3 films deposited at 350 °C. The Y_2O_3 films present bistable resistive switching characteristics for respective positive and negative voltage sweeps as shown in Fig. 12. The figure shows the typical unipolar resistive switching behaviors with both high resistance state (HRS) and low resistance state (LRS). The resistive switching from LRS (P1, N1) to HRS (P2, N2) and vice versa is independently realized under either a positive or a negative voltage sweep. For a LRS, the large current flows through the Y_2O_3 film at low voltage region and suddenly precipitates to a HRS at a reset voltage of about ±2 V. With an additional voltage sweep, the current keeps the path of HRS and then drastically increases at a set voltage of about ±5 V. The switching features are considered due to the formation and rupture of the conducting filaments through an insulating film.[40] The resistance ratio of HRS to LRS reading at 0.5 V is over 1,000 times, which is sufficient to distinguish two different digital signals as a non-volatile memory device.

Conclusions

We have successfully fabricated ALD-Y_2O_3 films approached by non-conventional liquid heteroleptic Y precursor, $(iPrCp)_2Y(iPr\text{-}amd)$ and have demonstrated its excellence through the materials characterization and the resistive switching memory device application. The novel $(iPrCp)_2Y(iPr\text{-}amd)$ has been synthesized with high yield and exist in a yellow oil at room temperature. The vapor pressure of $(iPrCp)_2Y(iPr\text{-}amd)$ at 168 °C is 1 Torr. This liquid begins to evaporate from 250 °C in a single step till 320 °C with very low residual mass. It also shows a thermal self-decomposition from 425 °C. Y_2O_3 film was successfully fabricated by thermal ALD using a liquid $(iPrCp)_2Y(iPr\text{-}amd)$ and water. The self-limited growth with a growth rate of 0.06 nm/cycle at 350 °C. The ALD window is 350-450 °C which a relatively high temperature. The crystalline Y_2O_3 film shows preferred (222) parallel to Si substrate surface. The chemical state of deposited Y_2O_3 film shows stoichiometric and constant composition through depth. From the XPS peak analysis for Y and O, it is observed negligible -OH contamination in whole film without any additional annealing or capping processes. The optical and dielectric constant are relatively high with the value of refractive index over 1.8 and dielectric constant of 24. The Ru/Y_2O_3/Ru resistor shows resistance switching between low and high resistance states with voltage sweeping and the resistance ratio between two states at 0.5 V is over 1,000 times.

Acknowledgements

This work was supported by Basic Science Research Program (2009-0083540, 2012R1A6A1029029) and Nano·Material Technology Development Program (2012M3A7B4034985) through the National Research Foundation of Korea (NRF) funded by the Ministry of Education and by the Ministry of Science, ICT & Future Planning.

Notes and references

[a] Division of Materials Science and Engineering, Hanyang University, Seoul 133-791, Korea. E-mail: jhahn@hanyang.ac.kr; Fax: +82-2291-1130; Tel:+82-2-2220-0407

[b] Institute of Nano Science and Technology, Hanyang University, Seoul 133-791, Korea

[c] Department of Nano and Electronic Physics, Kookmin University, Seoul 136-702, Korea

[c] Air Liquide Laboratories Korea, Seoul 120-749, Korea

† Electronic Supplementary Information (ESI) available. See DOI: 10.1039/b000000x/

1 G. D. Wilk, R. M. Wallace and J. M. Anthony, *J. Appl. Phys.*, 2001, **89**, 5243-5275.
2 Z. Wang, H. Xu, Z. Zhang, S. Wang, L. Ding, O. Zeng, L. Yang, T. Pei, X. Liang, M. Gao and L.-M. Peng, *Nano Lett.* 2010, **10**, 2024-2030.
3 T.-M. Pan, K.-M. Chen and C.-H. Lu, *Electrochem. Solid-State Lett.* 2011, **14**, H27-H29.
4 T.-M. Pan, L.-C. Yen, S. Mondal, C.-T. Lo and T.-S. Chao, *ECS Solid-State Lett.* 2013, **2**, P83-P85.
5 C. Grivas and R. W. Eason, *J. Phys.: Condens. Matter* 2008, **20**, 264011/1-264011/6.
6 T. Sanamyan, M. Kanskar, Y. Xiao, D. Kedlaya and M. Dubinskii, *Opt. Express*, 2011, **19**, A1082-A1087.
7 Z. Hou, G. Li, H. Liana and J. Lin, *J. Mater. Chem.*, 2012, **22**, 5254-5276.
8 Q. Dai, M. E. Foley, C. J. Breshike, A. Lita and G. F. Strouse, *J. Am. Chem. Soc.* 2011, **133**, 15475-15486.
9 K. Matsumoto and P. Mele, *Supercond. Sci. Technol.* 2011, **23**, 014001/1-014001/12.
10 Z. Fan, C.-C. Chao, F. Hossein-Babaei and F. B. Prinz, *J. Mater. Chem.*, 2011, **21**, 10903-10906.
11 J. H. Shim, C. C. Chao, H. Huang and F. B. Prinz, *Chem. Mater.* 2007, **19**, 3850-3854.
12 E. Ballée, A. Ringuedé, M. Cassir, M. Putkonen and L. Niinistö, *Chem. Mater.* 2009, **21**, 4614-4619.
13 L. Chen, C.-C. Lin, C.-W. Yeh and R.-S. Lie, *Materials* 2010, **3**, 2172-2195.
14 O. Lupan, B. Viana, T. Pauporté, M. Dhaouadi, F. S. Pellé, L. Devys and T. Gacoin, *J. Phys. Chem. C* 2013, **117**, 26768-26775.
15 J.-H. Lee, W. Y. Leung, J. Ahn, T. Lee, I.-S. Park, K. P. Constant and K.-M. Ho, *Appl. Phys.Lett.*, 2007, **90**, 151101.

16 S. M. George, *Chem. Rev.* 2010, **110**, 111-131.
17 V. Miikkulainen, M. Leskelä, M. Ritala and R. L. Puurunen, *J. Appl. Phys.* 2013, **113**, 021301/1-021301/101.
18 M. Cassir, A. Ringuedé and L. Niinistö, *Mater. Chem.*, 2010, **20**, 8987-8993.
19 S. B. Lee, I.-S. Park, Y.-M. Kim, S. J. Yoo, J.-G. Kim, H. N. Han and D. N. Lee, *Acta Materialia*, 2014, **66**, 97-104
20 M. Putkonen, T. Sajavaara, L.-S. Johansson and L. Niinistö, *Chem. Vap. Dep.* 2001, **7**, 44-50.
21 P. Myllymäki, M. Nieminen, J. Niinistö, M. Putkonen, K. Kukli and L. Niinistö, *J. Mater. Chem.* 2006, **16**, 563–569.
22 M. Putkonen, T. Sajavaara, J. Niinistö, L.-S. Johansson and L. Niinistö, *J. Mater. Chem.* 2002, **12**, 442-448.
23 T. Pilvi, E. Puukilainen, F. Munnik, M. Leskelä and M. Ritala, *Chem. Vap. Dep.* 2009, **15**, 27-32.
24 P. de Rouffignac, J.-S. Park and R. G. Gordon, *Chem. Mater.* 2005, **17**, 4808-4814.
25 J. Niinistö, M. Putkonen and L. Niinistö, *Chem. Mater.* 2004, **16**, 2953-2958.
26 P. Majumder, G. Jursich, A. Kueltzo and C. Takoudis, *J. Electrochem. Soc.* 2008, **155**, G152-G158.
27 P. Majumder, G. Jursich and C. Takoudis, *J. Appl. Phys.* 2009, **105**, 104106/1-104106/6.
28 R. Xu, S. K. Selvaraj, N. Azimi and C. G. Takoudis, *ECS Trans.* 2012, **50**, 107-116.
29 J. Niinistö, T. Hatanpaa, M. Kariniemi, M. Mantymaki, L. Costelle, K. Mizohata, K. Kukli, M. Ritala and M. Leskelä, *Chem. Mater.* 2012, **24**, 2002-2008.
30 T. Blanquart, J. Niinistö, M. Gavagnin, V. Longo, V. R. Pallem, C. Dussarrat, M. Ritala and M. Leskelä, *Chem. Mater*. 2012, **24**, 3420-3424.
31 P. A. W. van der Heide, *J. Elec. Spec. Rel. Phenom.* 2006, **151**, 79-91.
32 A. V. Naumkin, A. Kraut-Vass, S. W. Gaarenstroom and C. J. Powell, NIST X-ray Photoelectron Spectroscopy Database 20, 2012.
33 T.-M. Pan and J.-D. Lee *J. Electrochem. Soc.* 2007, **154**, H698-H703.
34 T. T. Van and J. P. Chang, *Surf. Sci.* 2005, **596**, 1-11.
35 J. Tao and M. Batzill, *Surf. Sci.* 2011, **605**, 1826-1833.
36 C. Durand, C. Doubourdieu, C. Vallée, V. Loup, M. Bonavalot, O. Joubert, H. Roussel and O. Renault, *J. Appl. Phys*. 2004, **96**, 1719-1729.
37 Z. M. Wang, J. X. Wu, Q. Fang and J.-Y. Zhang, *Appl. Surf. Sci.* 2005, **239**, 464-469.
38 J. Wang, T. Zhan, G. Huang, X. Cui, X. Hu and Y. Mei, *Opt. Express* 2012, 20, 18555-18567.
39 C. Durand, C. Dubourdieu, C. Vallée, E. Gautier, F. Ducroquet, D. Jalabert, H. Roussel, M. Bonvalot and O. Joubert, *J. Electrochem. Soc.*, 2005, **152**, F217-225.
40 I.-S. Park, K.-R. Kim, S. Lee and J. Ahn, *Jpn. J. Appl. Phys.*, 2007, 46, 2172-2174.